nature plants

Article

https://doi.org/10.1038/s41477-022-01274-z

Genome-wide dissection of changes in maize root system architecture during modern breeding

In the format provided by the authors and unedited

Supplementary information

Supplementary Note

Correlation analysis and principal component analysis of eight root traits

We divided the eight root traits into three categories based on cluster analysis: root angle (ROA, RTA, RBA), root width (RMEW, RMAW, ROIW), and root area (AREA, ACH) (Supplementary figure 1a and Supplementary figure 1b). The best linear unbiased prediction (BLUP) value for each trait was estimated across two locations and two years. Pearson's correlation analysis showed that most of the pairwise correlations between root traits were significant (r = 0.364–0.967, P < 0.001; Extended Data figure 1 and Supplemental Table 3). Through further principal component analysis (PCA), we found that the first two principal components (PCs) explained 93.29% of the phenotypic variation. The first PC was composed of root system traits related to angle and width; it explained 82.45% of the total phenotypic variation in RSA and represented the horizontal expansion of the root system as a whole. The second PC was related to the projected area of the root system; it explained 10.84% of the variation in RSA and represented the size of the root system as a whole (Extended Data figure 2). This analysis shows that the angle and width of root expansion in the horizontal direction is an important driver of differences in maize root system architecture.

Cluster analysis of 380 maize inbred lines and comparison of root architecture between different subpopulations

A cluster analysis of 380 maize inbred lines based on three representative traits (ROA, RMEW, and AREA) revealed that the association panel could be divided into three groups (Extended Data Figure 3a). As shown in Extended Data Figure 3b,c, group 1 (represented by CHANG7-2 and B73) showed smaller root angles, widths, and areas. Group 2 (represented by ZHENG58 and SI273) was characterized by medium root angles, widths, and areas. And group 3 (represented by MO17 and GEMS25) had large root angles, widths, and areas. We then compared root system architecture among the four subpopulations in the association panel; the SS subpopulation exhibited smaller root angles, widths, and areas (Extended Data Figure 3d). Consistent with this result, group 1 contained a higher proportion of lines from the SS subgroup (Extended Data Figure 3e). Clearly, germplasm resources with different genetic backgrounds have different RSA characteristics.

Supplementary Figures

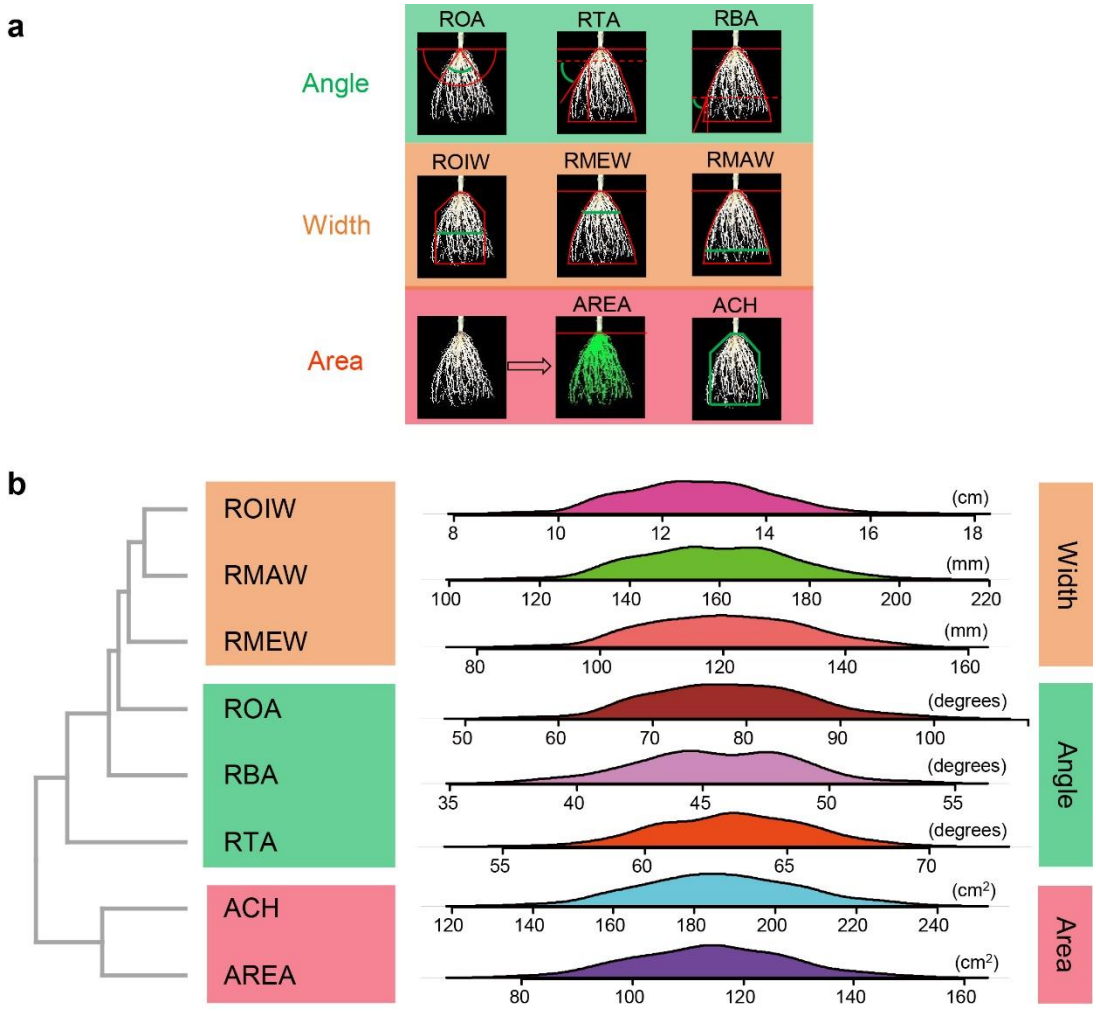

Supplementary Figure 1 Phenotypic variability of root system architectural traits in the GWAS panel.

(**a**) Diagram of root system architectural traits measured in our study. Root angle traits: ROA, RTA, and RBA (in green); root width traits: ROIW, RMEW, and RMAW (in yellow); and root area traits: AREA and ACH (in pink). (**b**) Root phenotype clustering of eight root traits and their distributions. The branch length represents the Euclidean distance. Abbreviation of eight root traits: opening root angle (ROA), top root angle (RTA), bottom root angle (RBA), median width of the root system (RMEW), maximum width of the root system (RMAW), root width after correction (ROIW), projected root area (AREA), and area of the root convex hull (ACH).

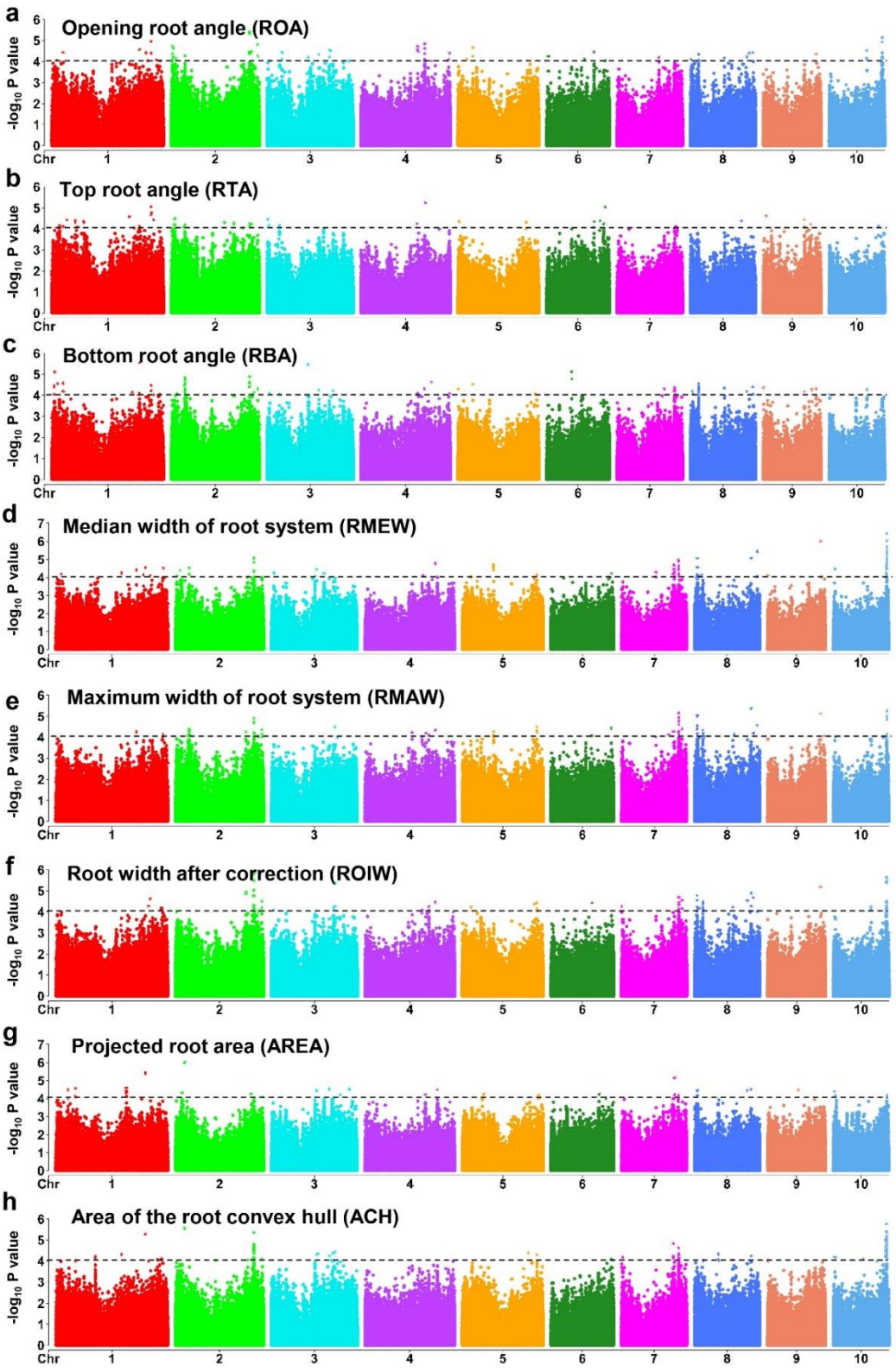

Supplementary Figure 2 Manhattan plots of eight root traits in the GWAS analysis. (**a**–**h**) are Manhattan plots of ROA, RTA, RBA, RMEW, RMAW, ROIW, AREA, and ACH. The horizontal axis shows the 10 chromosomes of the maize genome, and the vertical axis shows the $-\log_{10} P$ value. The P value was calculated in TASSEL 5.0 software using the compressed mixed linear mixed (CMLM) model. The dashed line indicates the significance threshold of $P = 1.0\times 10^{-4}$.

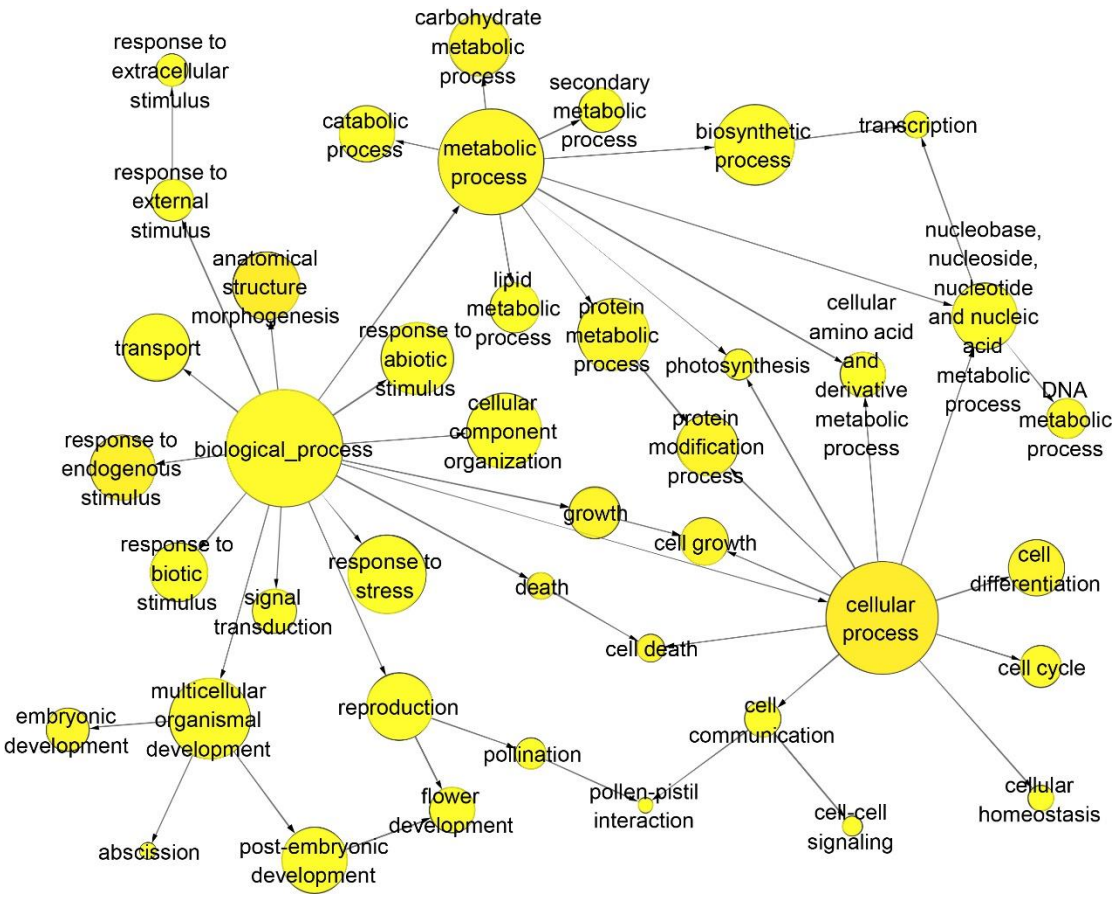

Supplementary Figure 3 GO enrichment analysis of 795 GWAS candidate genes. Node size represents the number of genes in the node, and node color represents the *P* value. *P* values were calculated using the R package topGO (https://bioconductor.org/packages/release/bioc/html/topGODESeq2.html).

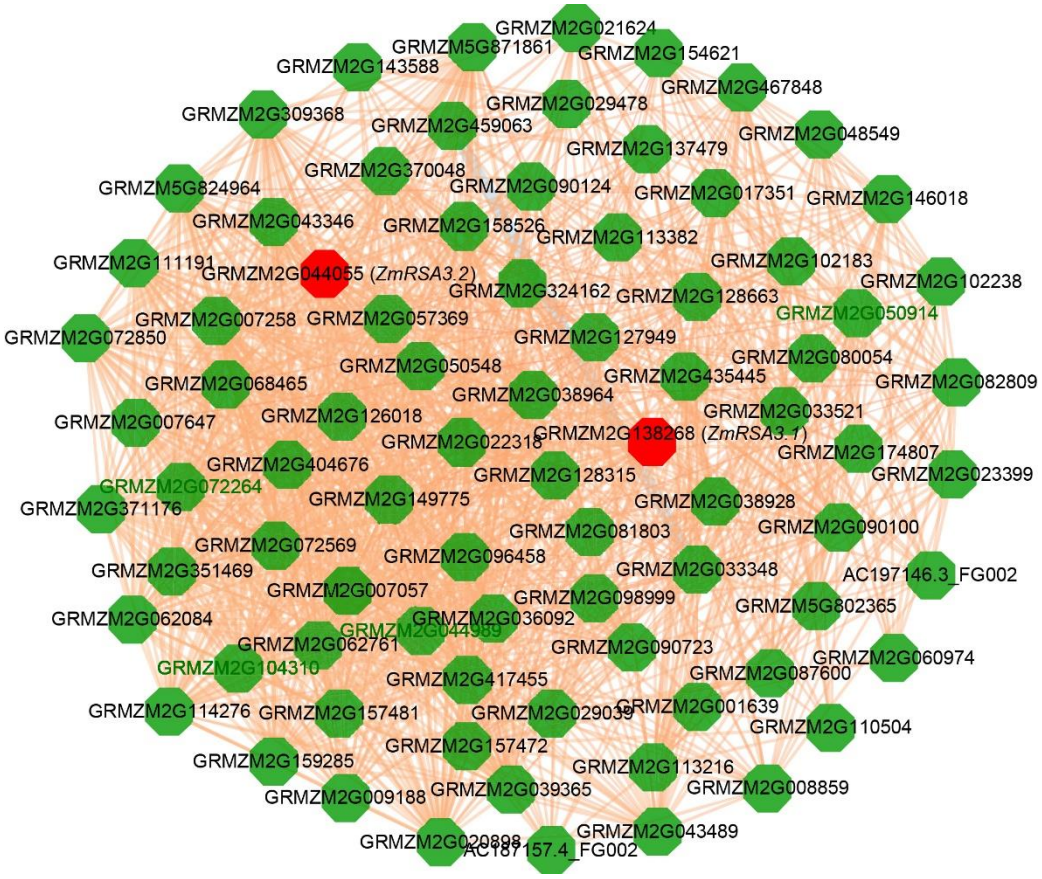

Supplementary Figure 4 Co-expression network analysis.

Candidate genes selected based on co-expression analysis. The red hexagons highlight two high-priority candidate genes (*ZmRSA3.1*: GRMZM2G138268; *ZmRSA3.2*: GRMZM2G044055) that are predicted to be strongly related to maize root development based on their gene annotations and published literature.

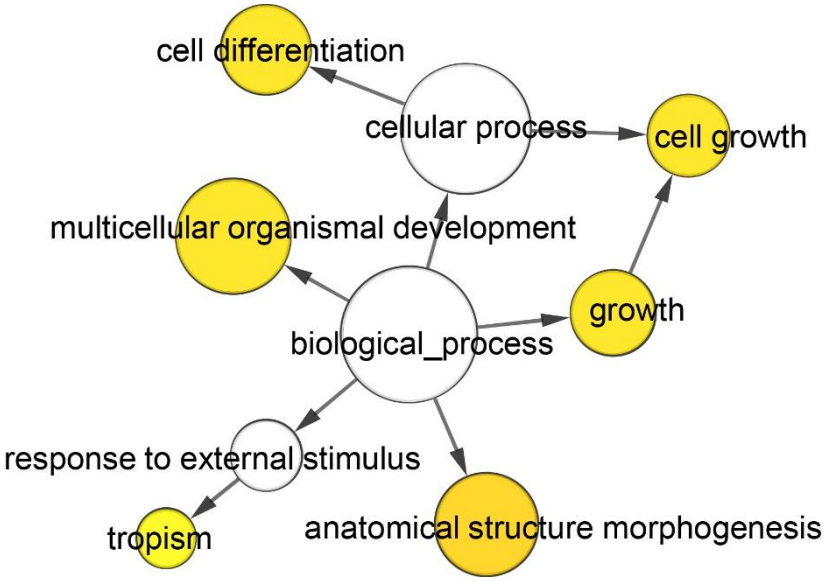

Supplementary Figure 5 GO enrichment analysis of 81 high-priority candidate genes selected based on co-expression network analysis. Node size represents the number of genes in the node, and node color represents the *P* value. *P* values were calculated using the R package topGO (https://bioconductor.org/packages/release/bioc/html/topGODESeq2.html).

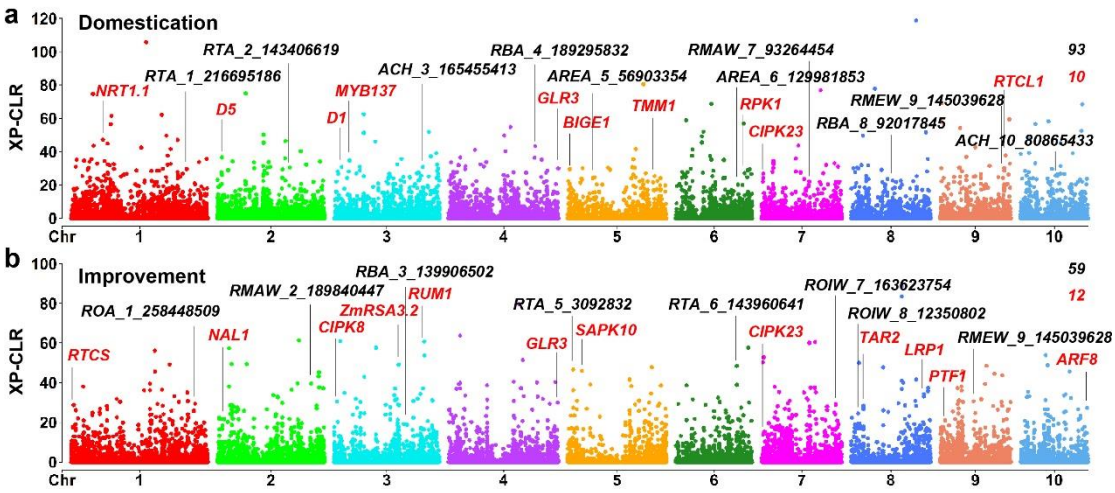

Supplementary Figure 6 Profiling of selective sweeps during maize domestication, improvement, and modern breeding.

(**a**) Genome-wide selective signals (XP-CLR score) during domestication (teosinte versus maize landraces) and improvement (landraces versus improved lines). (**b**) Genome-wide selective signals (XP-CLR score) during improvement (landraces versus improved lines). The genes marked in red are known root-related genes that have been functionally characterized, and the GWAS loci mapped in this study are marked in black. The black number at the upper left of each Manhattan plot is the number of GWAS candidate genes selected during domestication or improvement, and the red number is the number of GWAS candidate genes related to root development that have been functionally characterized.

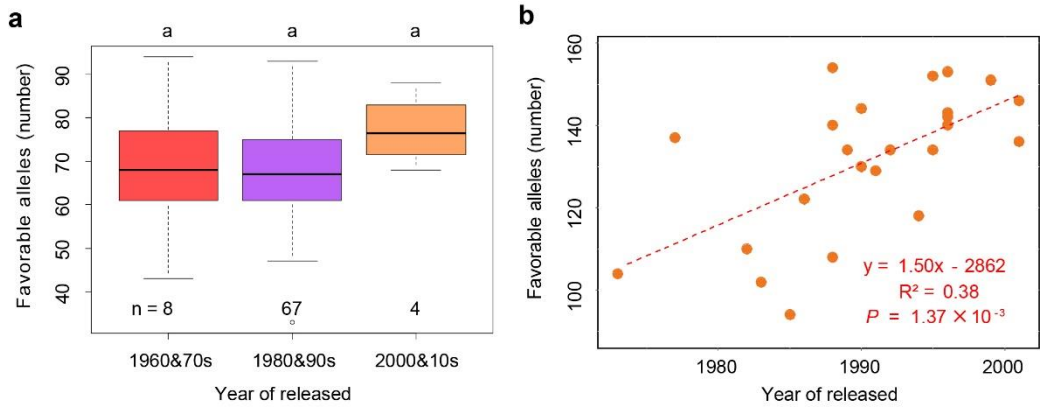

Supplementary Figure 7 Changes in the numbers of favorable alleles related to known root-related genes and high-priority candidate genes during the modern breeding process.

(**a**) The number of favorable alleles related to steep root architecture in maize inbred lines released in different breeding eras. 1960&70s (n=8), 1980&90s (n=67), and 2000&10s (n=4). In each box, the lower and upper boundaries represent the 25th and 75th percentiles, respectively. The middle horizontal line represents the median. The whiskers represent 1.5× the interquartile range. Same letters 'a' above the boxes indicate no significant differences at $P > 0.05$ (one-way analysis of variance followed by Duncan's multiple-comparison test). (**b**) The number of favorable alleles corresponding to maize hybrids selected from the inbred lines (n=27) in our association panel. The x-axis represents the release years of hybrids produced by crosses between inbred lines in the association panel. The y-axis is the number of favorable alleles related to steep root architecture identified by GWAS of eight root traits. Linear regression was used for the analysis, and the coefficient of determination (R^2) and P value of the resulting equation are provided.

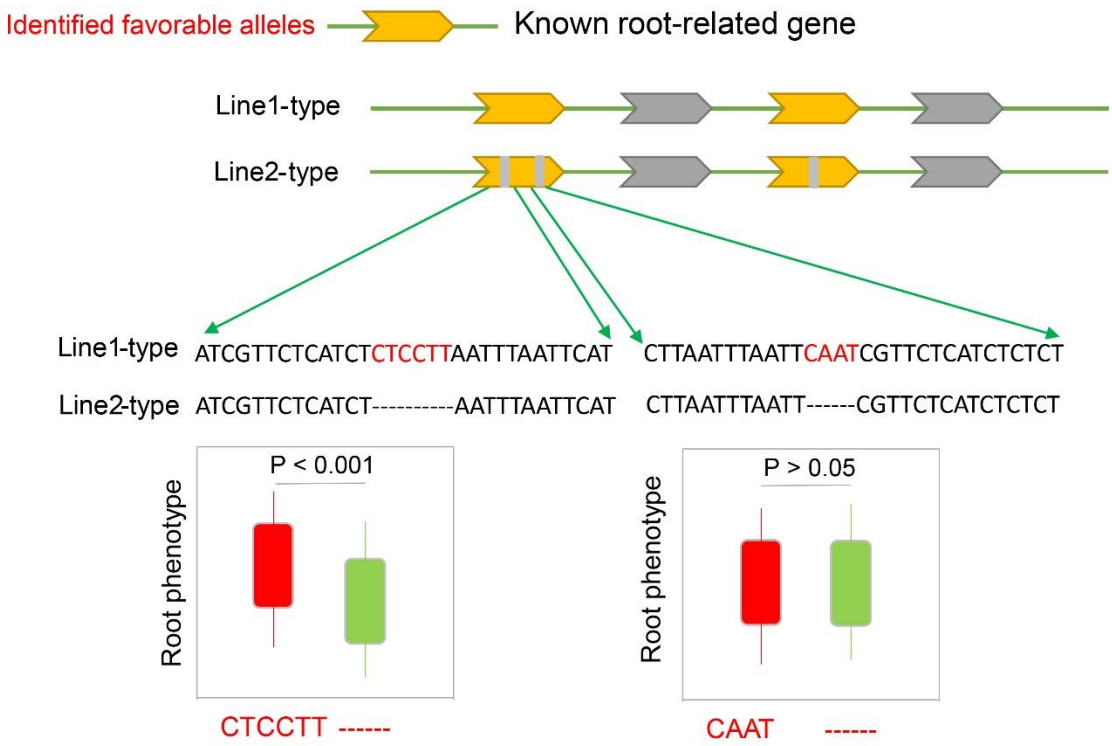

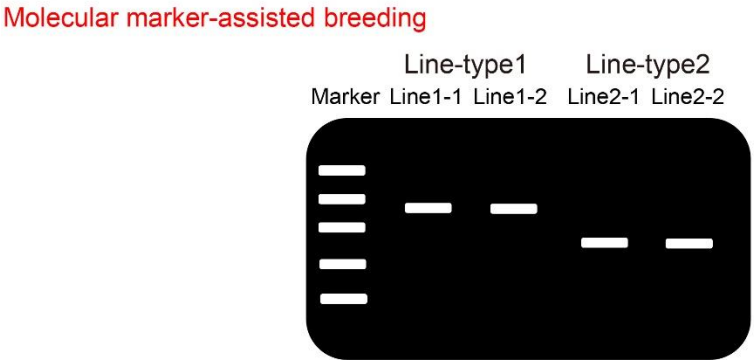

Supplementary Figure 8 Model of maize root genetic improvement based on favorable alleles for molecular marker-assisted breeding.

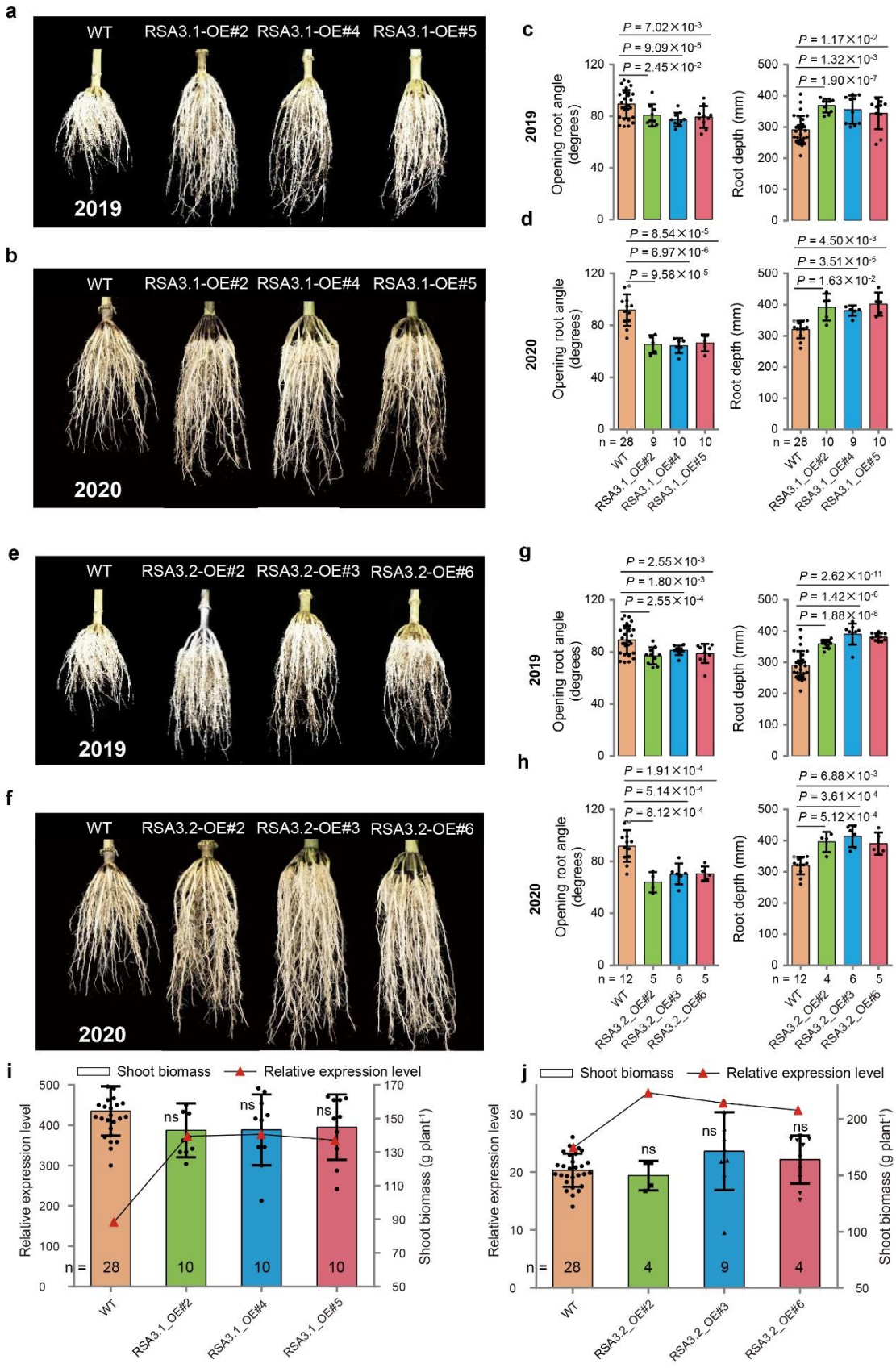

Supplementary Figure 9 Validation of two high-priority candidate genes associated with maize root architecture and shoot biomass.

(**a**) and (**b**) show the root architectures of wild-type and *ZmRSA3.1* overexpression plants in 2019 and 2020. (**c**) and (**d**) show the statistical analysis of the opening root angle (ROA) and root depth (DEPTH) values from wild-type and *ZmRSA3.1* overexpression plants in 2019 and 2020. (**e**) and (**f**) show the root architectures of wild-type and *ZmRSA3.2* overexpression plants in 2019 and 2020. (**g**) and (**h**) show the statistical analysis of ROA and DEPTH values from wild-type and *ZmRSA3.2* overexpression plants in 2019 and 2020. (**i**) and (**j**) show the statistical analysis of relative expression level and shoot biomass values from wild-type and overexpression plants of *ZmRSA3.1* and *ZmRSA3.2*, respectively. The 'n' in (**c**), (**d**), (**g**), (**h**), (**i**), and (**j**) indicates the number of biologically independent samples. The 'ns' in (**i**) and (**j**) indicates that there is no significant difference between the overexpression lines and the wild-type. Bars represent mean values ± SE. The *P* values of two-tailed Student's *t*-tests are indicated.

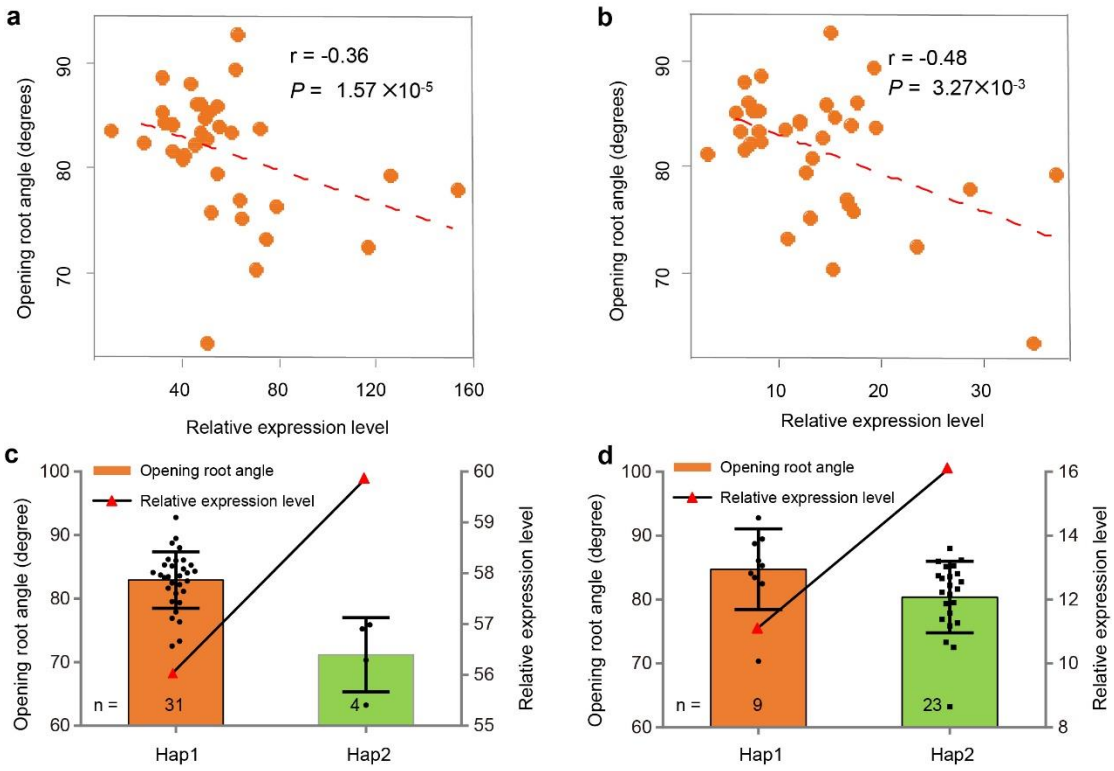

Supplementary Figure 10 The correlation of the opening root angle (ROA) with expression levels of *ZmRSA3.1* and *ZmRSA3.2*.

(**a**) and (**b**) show the correlation of the ROA with expression levels of *ZmRSA3.1* and *ZmRSA3.2*, respectively. (**c**) and (**d**) show the relationship between gene expression levels and ROA of *ZmRSA3.1* and *ZmRSA3.2* corresponding to two haplotypes, respectively. Gene expression levels are derived from the root transcriptome sequencing of 35 inbred lines (see Methods). Data are presented as mean values ± SD. The "n" in (**c**) and (**d**) indicates the number of inbred lines corresponding to different haplotypes. The *P* values in **a** and **b** are derived from two-sided Student's *t*-tests.

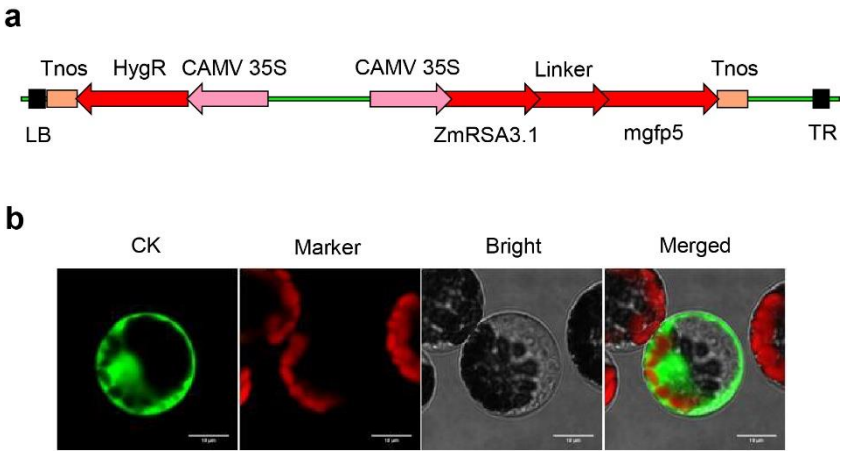

Supplementary Figure 11 Subcellular localization assay of ZmRSA3.1.

(**a**) Vector construction for subcellular localization assay. (**b**) Images of the empty vector control in maize mesophyll protoplasts. Representative images are shown. One times experiment was conducted. Scale bars = 10 μm.

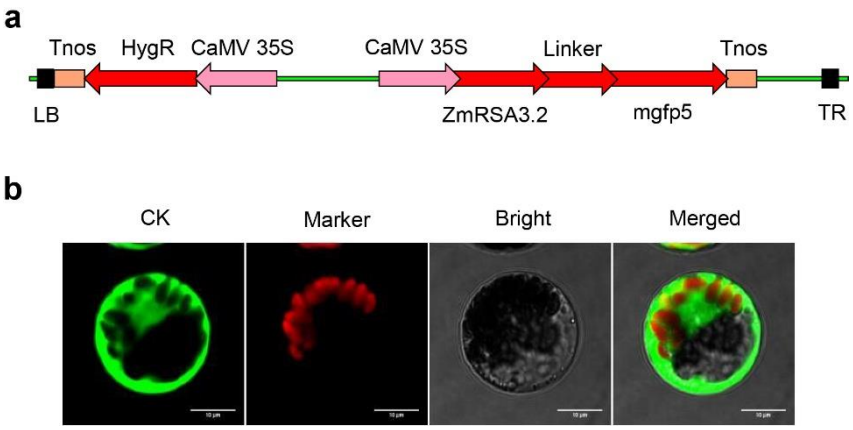

Supplementary Figure 12 Subcellular localization assay of ZmRSA3.2.

(**a**) Vector construction for subcellular localization assay. (**b**) Images of the empty vector control in maize mesophyll protoplasts. Representative images are shown. One times experiment was conducted. Scale bars = 10 μm.

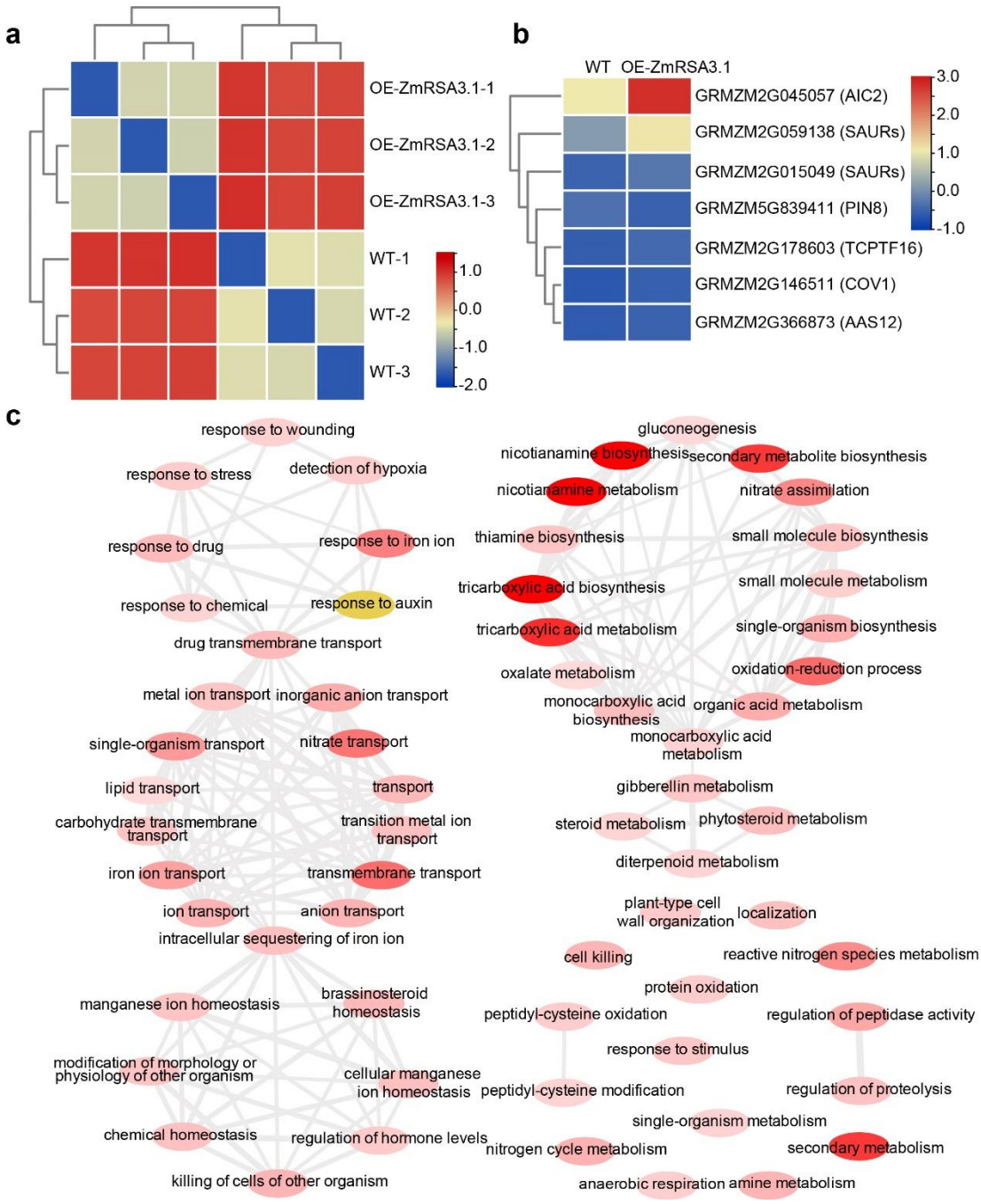

Supplementary Figure 13 Functional enrichment analysis of genes differentially expressed between the roots of wild-type and *ZmRSA3.1* overexpression lines.

(**a**) Pearson correlation coefficients and clustering analysis of the RNA-seq libraries. (**b**) Changes in the expression levels of genes related to the auxin signaling pathway in roots caused by overexpression of *ZmRSA3.1*. The color scale bars represent the result of processing the FPKM value centered on zero. (**c**) Gene Ontology enrichment analysis of genes differentially expressed between *OE-ZmRSA3.1* and the wild type. Node colors in (c) indicate the degree of enrichment from lower (light pink) to higher (red). Auxin-related enrichment results are marked in yellow.

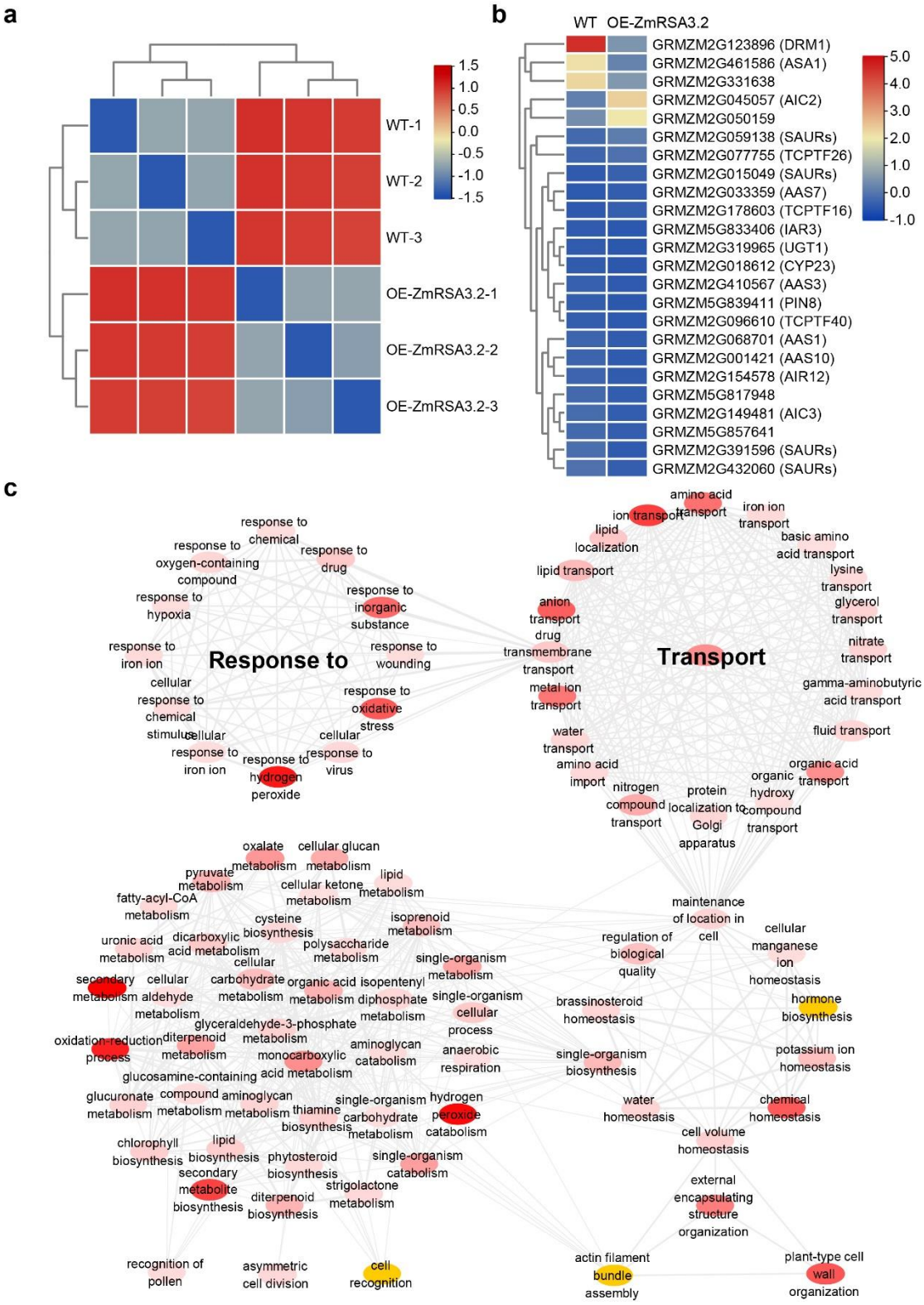

Supplementary Figure 14 Functional enrichment analysis of genes differentially expressed between the roots of wild-type and *ZmRSA3.2* overexpression lines.

(**a**) Pearson correlation coefficients and clustering analysis of the RNA-seq libraries. (**b**) Changes in the expression levels of genes related to the auxin signaling pathway in roots caused by overexpression of *ZmRSA3.2*. The color scale bars represent the result of

processing the FPKM value centered on zero. (**c**) Gene Ontology enrichment analysis of genes differentially expressed between *OE-ZmRSA3.2* and the wild type. Node colors in (c) indicate the degree of enrichment from lower (light pink) to higher (red). Enrichment results related to hormone pathways and closely related to the function of *ZmRSA3.2* are marked in yellow.

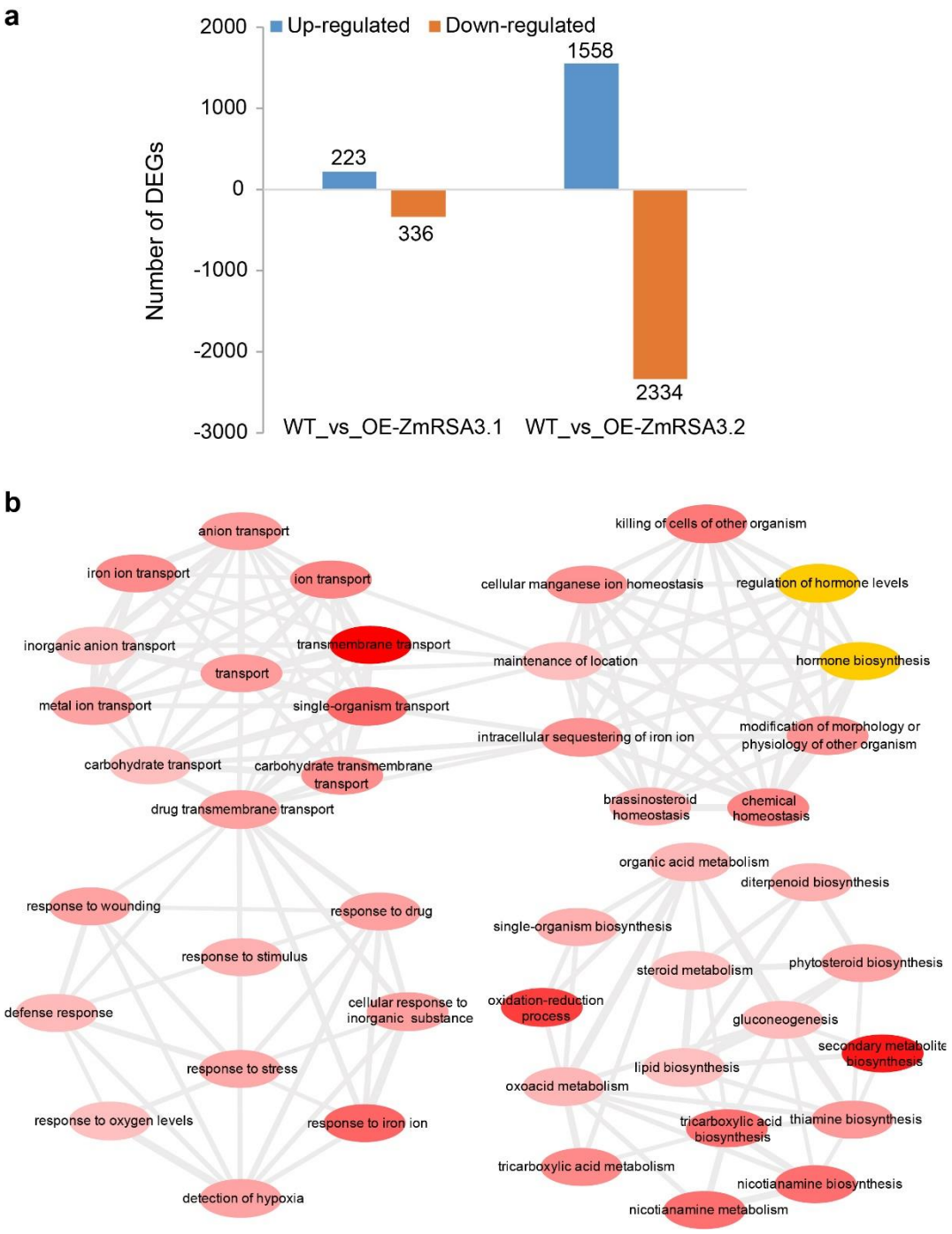

Supplementary Figure 15 Differentially expressed genes between OE-ZmRSA3.1, OE-ZmRSA3.2, and the wild type.

(**a**) The number of upregulated and downregulated genes between the wild type and *OE-ZmRSA3.1* (left) and *OE-ZmRSA3.2* (right). (**b**) Gene Ontology enrichment map of common DEGs between *OE-ZmRSA3.1* and *OE-ZmRSA3.2*. Node colors in (c) indicate the degree of enrichment from lower (yellow) to higher (red). Hormone-related enrichment results are marked in yellow.

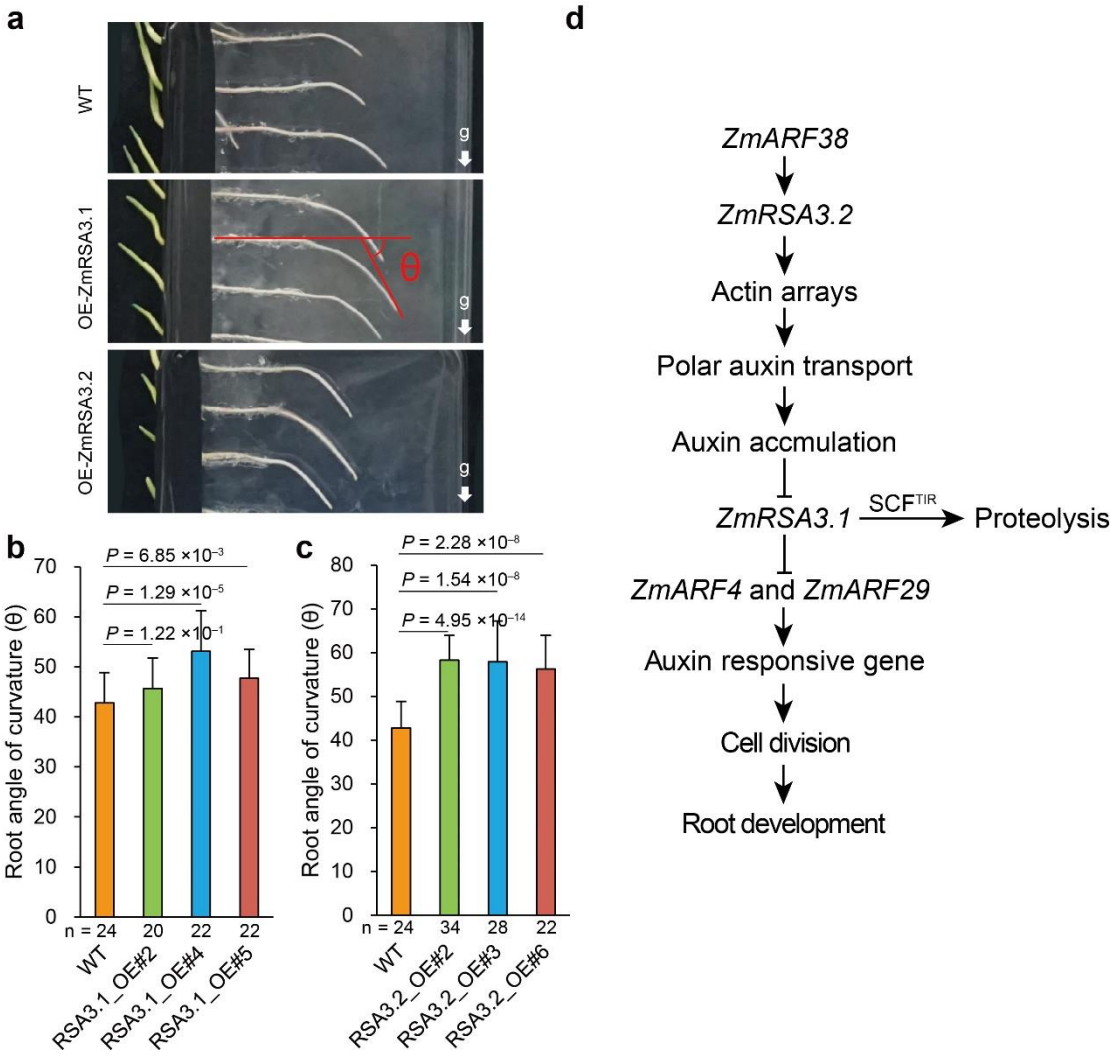

Supplementary Figure 16 Effect of ZmRSA3.1 and ZmRSA3.2 overexpression on root gravitropic curvature and a proposed working model of the means by which *ZmRSA3.1* and *ZmRSA3.2* control maize root system development. (a) The root curvature angle (θ) after rotation of wild-type, ZmRSA3.1, and ZmRSA3.2 overexpression plants 4 days after sowing in agarose gel. (**b**) Statistical analysis of root curvature angle (θ) after rotation of wild-type and ZmRSA3.1 overexpression plants. (**c**) Statistical analysis of root curvature angle (θ) after rotation of wild-type and ZmRSA3.2 overexpression plants. Data are presented as mean values ± SD. The 'n' in (**b**) and (**c**) indicates the number of biologically independent samples. The *P* values of two-tailed Student's t-tests are indicated.

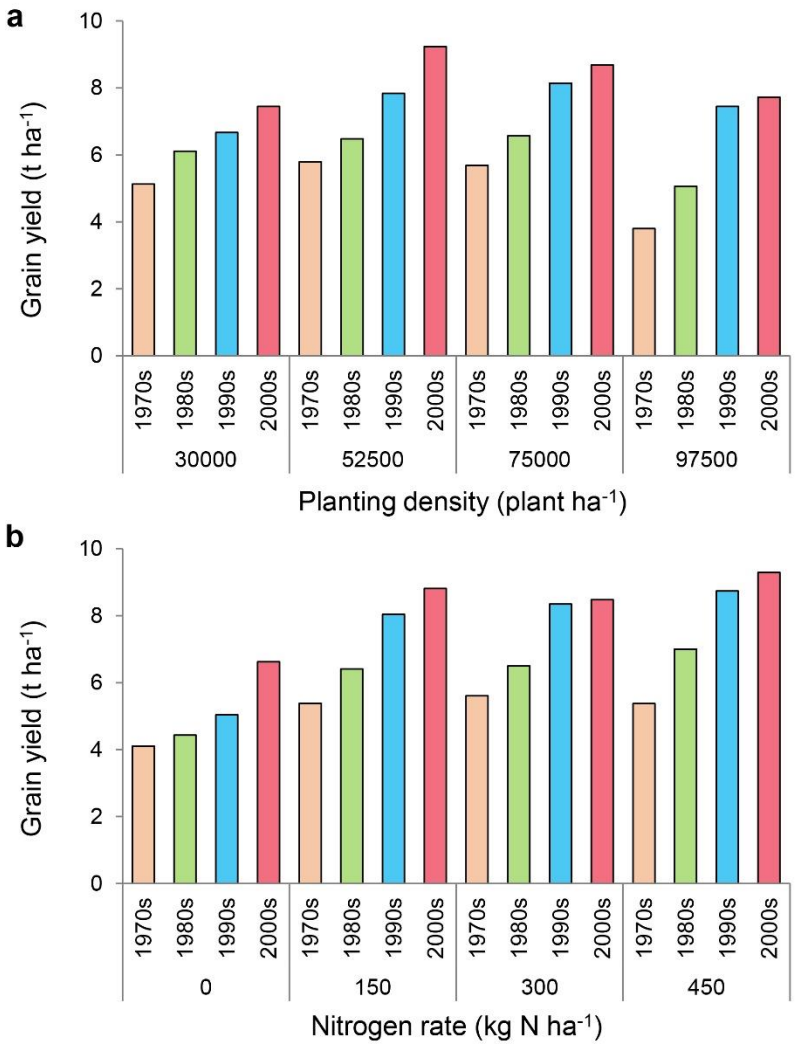

Supplementary Figure 17 Influence of planting density and nitrogen application rate on the grain yield of hybrid maize in different years (edited from Qian et al., 2012).

Reference: Qian, C.R., Yu, Y., Gong, X.J., Jiang, Y.B., Zhao, Y., Wang, J.H., Yang, Z.L., and Zhang, W.J. (2012). Response of Grain Yield to Plant Density and Nitrogen Application Rate for Maize Hybrids Released from Different Eras in Heilongjiang Province. *Acta Agronomica Sinica* 38, 1864–1874.

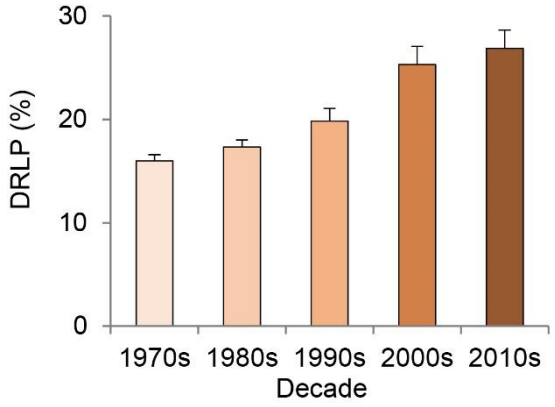

Supplementary Figure 18 The proportion of root length in the 20–50 cm soil layer (DRLP) for maize varieties released in different breeding eras.

The x-axis indicates the decades when the hybrids were released, and the y-axis is the percentage of deep root length to total root length (edited from Yu et al., 2019).

Reference: Yu, X.F., Wang, Y., Gao, J.L., Hu, S.P., Sun, J.Y., Wang, Z.G., and Li, X.L. (2019). Succession Law of Root Traits and Yield of Different Maize Varieties in Different Years and Its Response to Subsoiling. *Journal of Maize Sciences* 27, 134–140.

Supplementary Figure 19 Root sampling under field conditions.
(**a**) Three to five plants with relatively uniform growth were selected from each line for root excavation under field conditions. (**b**) The root system was sampled by digging a soil core (40 cm diameter × 30 cm depth) with the plant at the center. (**c–d**) Roots were clean using a pressure-adjustable high-pressure water gun. (**e–f**) Root image acquisition using a studio with stable LED lighting.